Mitigation of Switching Losses and Electro Magnetic Interference with Buck Converter for Renewable Energy Applications

K. V. Govardhan Rao[1] M. Kiran Kumar[1], B Srikanth Goud[2,‡], T. Anuradha Devi[3], Ch. Rami Reddy [4,5], Thulasi Bikku[6], Basem Alamri[7], Pidikiti Tripura[8], Ch Naga Sai Kalyan[9]

[1]Electrical and Electronics Engineering, Koneru Lakshmaiah Education Foundation, Vaddeswaram, Guntur, India-522302
[2]Electrical and Electronics Engineering, School of Engineering, Anurag University, Hyderabad, India-500088
[3]Electrical and Electronics Engineering, Vardhaman College of Engineering, Kacharam, Hyderabad, Telangana, India-501218
[4]Electrical and Electronics Engineering, Joginpally B R Engineering College, Hyderabad, India 500075
[5]Applied Science Research Center, Applied Science Private University, Amman 11937, Jordan
[6]Computer Science and Engineering, Amrita School of Computing Amaravati, Amrita Vishwa Vidyapeetham, Andhra Pradesh, 522503, India.
[7]Department of Electrical Engineering, College of Engineering, Taif University, P.O. Box 11099, Taif 21944, Saudi Arabia
[8]Department of Electrical and Electronics Engineering, RVR & JC College of Engineering, Guntur, AP, India
[9]Department of Electrical and Electronics Engineering, Vasireddy Venkatadri International Technological University, Nambur, Guntur, AP, India-522 508
(kv.govardhanrao@gmail.com, kiran.malligunta@gmail.com, bsgoud07@gmail.com, anuradhadevi.eee@gmail.com, crreddy229@gmail.com, b_thulasi@av.amrita.edu, b.alamri@tu.edu.sa, tripura.pidikiti@gmail.com, kalyanchallapalli@gmail.com)
‡ Corresponding Author: B. Srikanth Goud, Electrical and Electronics Engineering, School of Engineering, Anurag University, Hyderabad, India-500088, India. E-Mail: bsgoud07@gmail.com

Received: 07.12.2023 Accepted: 14.01.2024

Abstract- Power electronics have made great strides forward for the implementation of soft switching in choppers, which resulted in significant improvements in efficiency, power density, EMI suppression, and physical size reduction. Over the past forty years, many different gentle switching methods have been documented. There are always drawbacks to using a hard-switching buck converter to transform PV energy. The conversion efficiency of a freewheeling diode is lowered by EMI, high switching losses, stresses, and reverse-recovery losses. A buck converter with soft-switching cells has been offered as a solution to these problems for using PV panels. The suggested buck converter makes use of a straightforward active process of soft switching consisting of passive elements like inductors, capacitors, and power electronic devices like MOSFET. Because of this, ZVS (zero-voltage switching) is possible with active switches. This allows for a significant decrease in EMI, active switch strain, and switching losses. Freewheeling diode reverse-recovery losses can be minimized by using a passive soft-switching cell made up of a passive element capacitor and two diodes. The suggested buck converter with soft-switching cells is implemented for renewable energy sources of PV panels, Fuel cells, and Battery applications and has been validated using simulation.

Keywords- Hard-switching, soft-switching technique, electromagnetic interference (EMI), zero-current-switching (ZCS), zero-voltage-switching (ZVS), solar PV; fuel cell; battery.

1. Introduction

Pollution of the environment and the formation of greenhouse effects on Earth are both caused by humans' excessive consumption of fossil fuels. The research and development of alternative energy sources as well as the mitigation of the effects of greenhouse gases have been significant topics [1]. Solar energy is the most popular form of renewable energy since it is the least disruptive to the environment, does not contribute to pollution, does not emit radioactive waste, and does not deplete resources [2]. Now, photovoltaic panels are used to effect the transformation of solar energy into electric power. PV panels have become increasingly common in power systems in recent years due to their extremely long lifespans and their adaptability as a kind of energy source. PV panels [3], on the other hand, have features that make them unstable and intermittent, making it impossible for them to deliver a stable supply of power [4]. Therefore, photovoltaic (PV) panels typically need to contain a maximum power point tracking (MPPT) algorithm and a switching power converter to supply the load with DC power of good quality [5]. The development of switching power converters that can operate at high frequencies has been driven by research motivated by the desire for improved performance, reduced volume, and reduced weight [6-7]. There have been various non-isolated switching power converter developments and plans. Buck, Boost, Cuk, Zeta,

and Sepic converters are popular in low and medium-power applications due to their simple designs. Buck converters are used in non-isolated voltage-stepping applications [8]. Switching losses in the buck converter are caused by the active switch (MOSFET) hard-switching situation with a freewheeling diode return-recovery current. Therefore, buck converter has substantial power losses, EMI, and low conversion efficiency [9]. Figure 1 shows the active switch and freewheeling diode hard switching. EMI and power losses in the buck converter increase with switching frequency. Many soft-switching solutions have been proposed to address these concerns [10]. Soft switching reduces switching losses and EMI by improving power switch on/off switching.

The organization of the manuscript is, in section-1 described about the introduction and in section-2 classifications and procedures for soft switching with comparison tables of properties of converters and number of resonant elements used. In section-3 proposed buck converters with their modes of operation, in section-4 MPPT selection methods, and section-5, simulation results for PV, simulation results for Fuel cell, and simulation results of battery are explained finally in section-6 conclusion with glossary is mentioned.

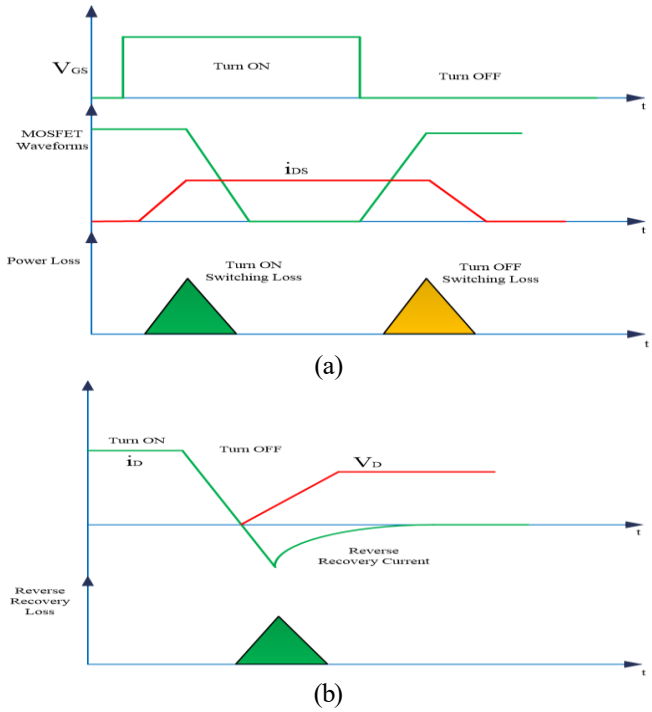


Fig. 1. Switching ON and switching OFF waveforms:(**a**) MOSFET; (**b**) diode.

2. Classification of Procedure of Soft Switching

In current years, more soft-switching methods have emerged. Figure 2 classifies soft-switching DC-to-DC converters [11]. Resonant inductors are usually large for load resonant procedures. This increases conduction loss due to high circulation energy. These methods also have higher current or voltage strains than resonant switch methods [12]. Resonant switch approaches fall into two main categories: active and passive soft switching. The two types of active soft-switching approaches are zero-voltage (ZVS) and zero-current (ZCS) [13].

2.1 Quasi-Resonant Converters (QRC)

The QRC has two extra parts that make it work: an inductor (Lr) and a capacitor (Cr). Whether the auxiliary element is linked in series, parallel, or both depends on how the converter is built or what it is used for. This can also connect the series-parallel connection to the load or turn on a converter. Everything is done to get ZVS, ZCS, ZVT, or ZCT on the diode or switch. How the switch and diode are linked to the reacting parts [14]. In this setup, the diode and switch can't soft-switch at the same time [15].

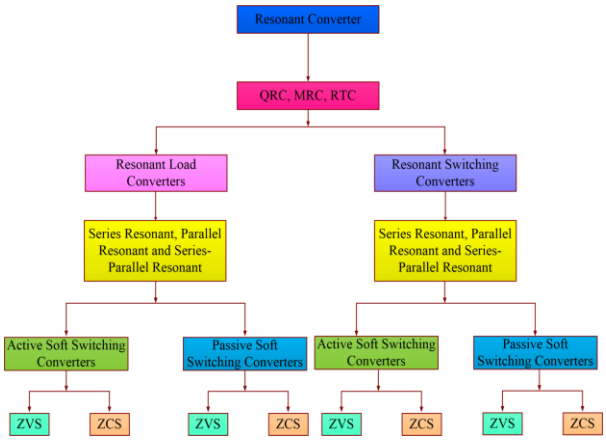


Fig. 2 Classifying DC-DC converters using soft switching.

No matter how easy the setup is or how little current it has on the switches. Also, the single-ended ZVS-QRC active switch has high voltage stress that changes with the load range. Because of this, they can be used in low-power situations. A high-rated device is needed for resonance peak voltage [16]. When the huge resonant inductor and the rectifier diode's parasitic junction capacitance work together, they make a lot of noise. In Figure 3(a), a resonant capacitor (Cr) is moved across the main switch of the ZVS-QRC. In Figure 3(b), the ZCS-QRC is shown with resonant inductors ($L1$, $L2$) linked in series with switches ($S1$, $S2$) to turn on the ZCS.

2.2 Multi-Resonant Converters (MRC)

According to research, MRCs are modified QRCs with many reactive components. Figure 4 shows two resonating inductors and one resonance capacitor as reactive elements. The symbols Ls, Lm and Cs represent these. There are two ways to connect devices for ZVS and ZCS. ZVS or ZCS can be offered for the diode and switch, depending on the operation mode. Thus, MRC are sometimes called double-ZVS or double-ZCS converters [17-19]. All semiconductor devices in ZVS- MRC switch at zero voltage.

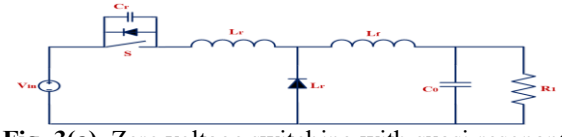


Fig. 3(a). Zero voltage switching with quasi-resonant.

Converter.

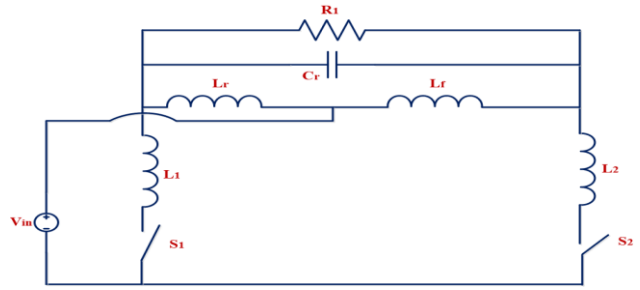


Fig. 3(b). Zero current switching with quasi-resonant converter.

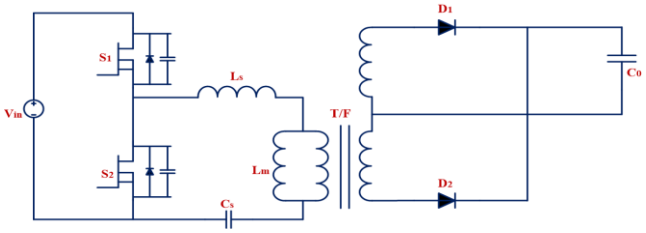


Fig. 4. Multi resonant converter with ZVS and ZCS.

Due to the high circulating current, this reduces switching and noise losses but increases conduction losses. Active and passive switches endure voltage and current strains as a result. These converters are suitable for high-frequency applications because they impose lower voltage and current strains than QRC.

2.3 Resonant Transition Converter (RTC) or Zero Transition Converters (ZTC)

Two resonance tanks (L and C) and two switches are the four extra parts that RTC uses. The RTC can make a zero-voltage transition (ZVT) or a zero-current transition (ZCT). ZCT stands for zero-current transitions and ZVT stands for zero-voltage changes. When there is no power, [20-23] ZCT turns off the main switch. When there is no voltage across the main switch, ZVT turns it on from off. Parts a and b of Figure 5 show ZCT and ZVT converters. The main things that affect ZTC are the hard auxiliary switch switching, the limited voltage conversion range, the high circulation current, the high peak current/voltage stress, and the higher conduction losses. RT PWM converters can lower the switch voltage to zero in near-boundary conduction mode by adding an extra RT phase.

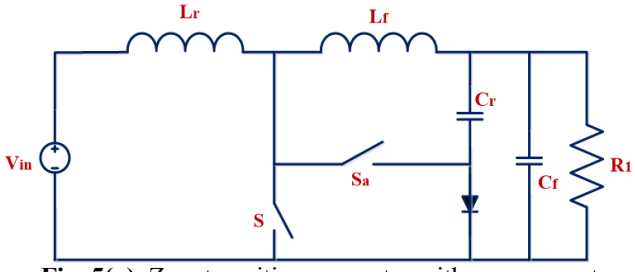


Fig. 5(a). Zero transition converter with zero current transition.

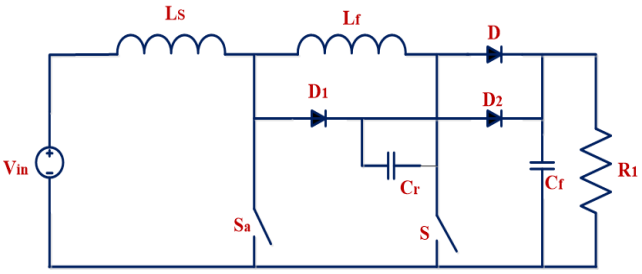


Fig. 5(b). Zero transition converter with zero voltage transition.

Most converters can only perform actual zero voltage switching (ZVS) within a voltage range [24-25]. This restricts their voltage range. Table 1 shows the main features, pros, and cons of QRC, MRC, and RTC circuit designs, along with their pressures and losses.

The resonant parts of soft-switching converter families are also shown in Table 2. This list shows how many extra parts (L, C) are in each family and what switch are used for them.

Table 1. Comparison of the main properties of QRC, MRC, and RTC

Converter Family	Voltage stress	Current stress	Conduction losses	Switching losses	Merit	Demerits	Application
QRC	An abnormally high potential stress that is proportional to the load potential	Very little strain in terms of current for the active switch	The high circulating current causes losses, which in turn leads to a decrease in power density and efficiency	The interplay of rectifier diodes, parasitic capacitance, and the massive resonant inductor results in severe switching noise.	Comparatively low number of components when compared to MRC and RTC converters.	Put a lot of weight on the frequency control; greater resonant peak voltage calls for a device with a higher rating.	Appropriate for use in applications requiring low power

MRC	As little voltage stress as possible on both the active and inactive switches compared to QRC	Current strain is not too great for either the active or the passive switch	An increase in conduction losses because of the smaller size of the filter and the reactive components	Decreased switching losses and operational noise	Control dynamics with a wider range, and every power switch uses ZVS.	There is a lot of voltage stress and a lot of flowing current because of the resonance effect of leakage inductance e and device parasitic capacitance	Suitable for high-frequency tasks, like those done by LCD or LED drivers, power supply chips for microprocessors ors or other units, and so on.
RTC	Stress caused by low voltage	Low current stress	An increase in the amount of conduction losses because of additional components	PWM Converters s have higher switching losses than other types of converters.	Exceptionally high- power density along with efficiency	Control system with a lot of moving parts. There is no smooth commutation while using the auxiliary switch. ZVS with a restricted range	Suitable for use in applications requiring high-power

Table 2. Based on the family of resonant converters, the number of resonant elements used

S. No	Family	Number of Resonant Capacitors	Number of Resonant Inductors	Auxiliary Switch	Number of Auxiliary elements
1.	QRC	One	One	Zero	Two
2.	MRC	One or two	One or two	Zero	Three
3.	RTC	One	One	Two	Four

3. Preferred Buck Converter

Figure 6 illustrates the structure of the preferred buck converter with the technique of soft switching [26-27] that will be used for applications using PV panels [28-29]. The photovoltaic panels shown in Figure 6 can be conceptualized as a source of continuous voltage for the sake of demonstration and investigation [30-32]. The PV panels are replaced with Fuel cells and batteries for their implementation of application [33]. Figure 7 displays it in a format that is a simplified circuit of the proposed one.

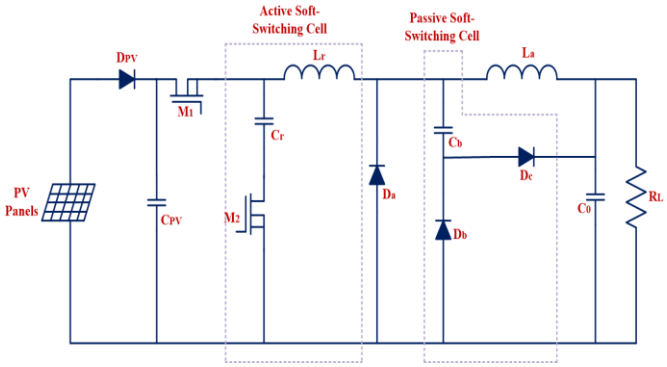


Fig. 6. Preferred buck converter with the technique of soft switching including PV application.

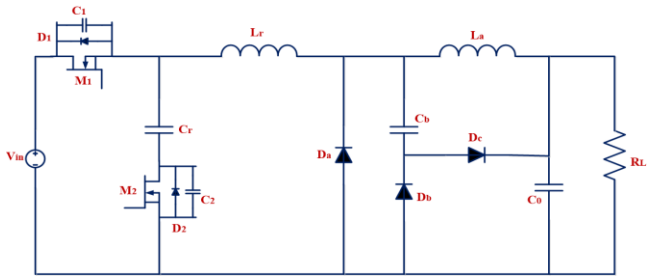


Fig. 7. Simplified circuit of proposed circuit here are some assumptions to simplify the operational mode explanation.

Here are some assumptions to simplify the operational mode explanation.

1. The body diodes ($D1$ *and* $D2$) and dependent capacitors ($C1$ *and* $C2$) of the main and secondary switches ($M1$ *and* $M2$) looked during steady-state operation to study ZVS characteristics.
2. All the components are ideal.

Figure 8 illustrates hypothetical waveforms of current and voltage for the essential components as well as the driving signal switches ($M1$ *and* $M2$) to make the operational principles easier to understand.

The proposed soft-switching buck converter has several operational modes, which will be detailed in turn:

Mode:1: $t_0 < t < t_1$

One switch, M_1, is on at time t_0, while the other, M_2, is off. There is a straight-line increase in the current going through the load R_L, resonant inductor L_r, buffer capacitor C_b, and diode D_c, so does its current i_{Lr}. This period sees a linear decline in storage inductors and load freewheeling diode current. The current via the resonant inductor i_{Lr} and storing inductor i_{La} can be represented as [1]:

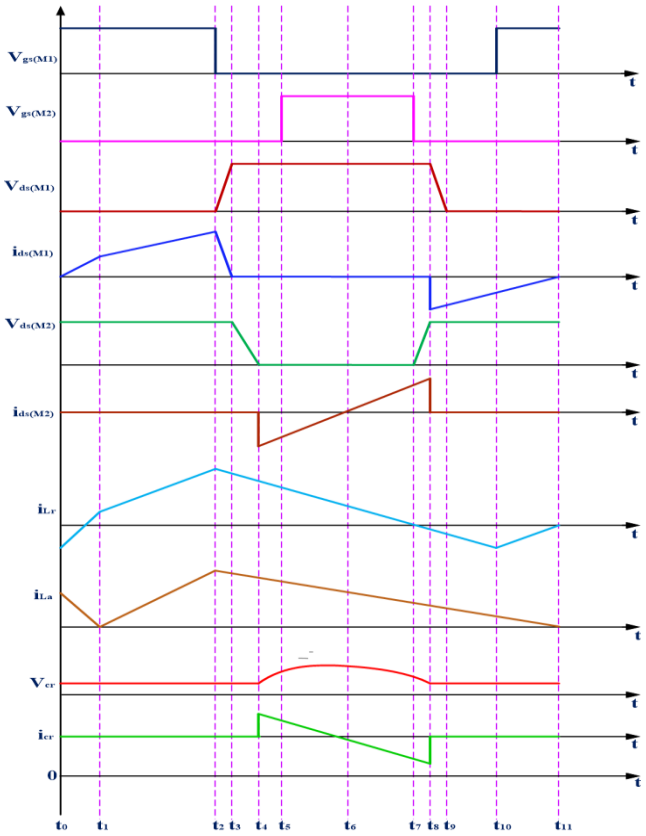


Fig. 8. Key component current and voltage waveforms of various modes in the preferred technique with soft-switching buck converter during a switching cycle.

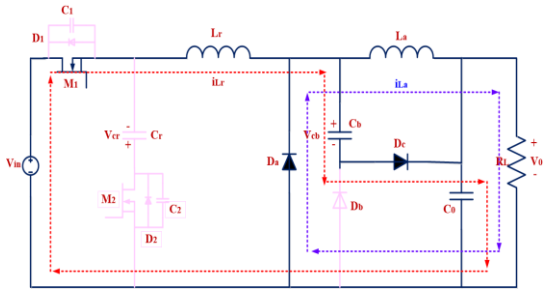


Fig. 9(a). Equivalent circuit of the proposed converter at Mode. 1.

$$i_{Lr} = \frac{V_{in} - (V_{cb} + V_0)}{L_r}(t - t_0) \quad (1)$$

$$i_{La} = \frac{V_0}{L_a}(t - t_0) \quad (2)$$

Mode 1's corresponding circuit is explained in Figure 9(a).

Mode: 2 : $t_1 < t < t_2$

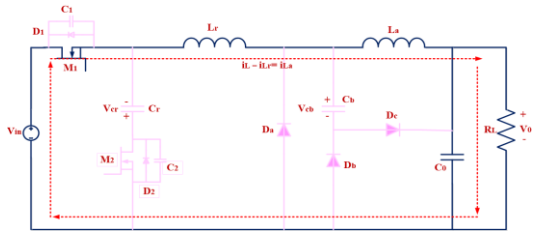


Fig. 9(b). Equivalent circuit of the proposed converter at Mode. 2.

At time t_1, the current in the resonant inductor, i_{Lr}, is the same as the current in the stored inductor, i_{La}. Also, the voltage of the buffer capacitor is charged to V_{La} plus Vo. In this way, the freewheeling diode D_a is turned off [18]. Now, i_L is:

$$i_{Lr} = \frac{V_{in}}{L_r + L_a}(t - t_1) \quad (3)$$

Where $i_L = i_{Lr} = i_{La}$

Figure. 9(b), represents the equivalent circuit of the proposed converter at Mode. 2

Mode: 3: $t_2 < t < t_3$

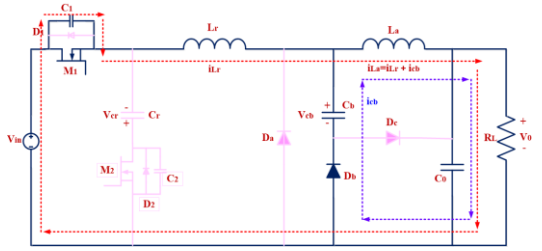


Fig. 9(c). Equivalent circuit of the proposed converter at Mode. 3.

The main switch M_1 is not working at time t_2, and neither is the secondary switch M_2. Along with the main switch M_1, a parasitic capacitor C_1 charges as the current i_{L1} rises slowly. Also, the stored in passive element inductor L_a, load R_L, and diode D_b all drain buffer capacitor C_b, which drains it. This is how the inductor current M_1 is shown [5]:

$$i_{La} = \frac{V_{in}}{L_r + L_a}(t - t_2) + i_{cb}(t - t_2) \quad (4)$$

Figure. 9(c), represents the equivalent circuit of the proposed converter at Mode. 3

Mode: 4 : $t_3 < t < t_4$

When time t_3 comes around, the buffer capacitor $C_b$goes down to zero, and drain-source capacitor V_{DS1} of the key switch M_1 goes up near $V_{in} - (V_{Lr} + V_{La} + V_0)$.

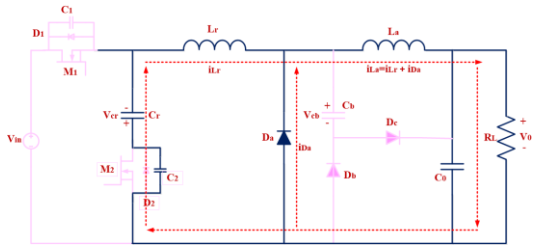


Fig. 9(d). Equivalent circuit of the proposed converter at Mode. 4.

This makes D_a, the uncontrolled diode, work. This current i_{La} has two sides. One side goes to the resonant inductor, and the other side goes to the freewheeling diode D_a. The resonant inductor L_r gives energy to C_2, which is the parasitic capacitance in secondary switch M_2. For the auxiliary switch M_2 to have a ZVS function [8], the resonant inductor's L_r energy must follow this inequality:

$$\frac{1}{2}[i_{Lr}(t-t_2)]^2 L_r > \frac{1}{2}[V_{DS2}(t-t_3)]^2 C_2 \quad (5)$$

Inductor current L_a

$$i_{La} = \frac{V_0}{L_a}(t-t_3) \quad (6)$$

Figure. 9(d), represents the equivalent circuit of the proposed converter at Mode. 4

Mode 5: $t_4 < t < t_5$

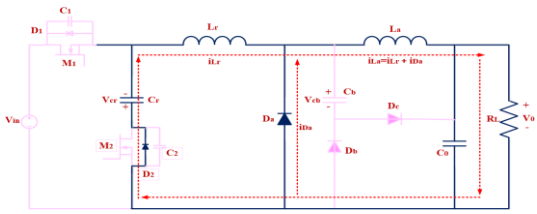


Fig. 9(e). Equivalent circuit of the proposed converter at Mode. 5.

At time t_4, the voltage through the extra switch M_1 drops to zero. A ZVS feature is made when current i_{Lr}flows through the resonant inductor and makes the diode D_2 of the assisting switch M_2 conduct. These are some ways to show the resonant and stored inductor currents [21], i_{Lr} and i_{La}:

$$i_{Lr} = \frac{V_{cr}}{L_r}(t-t_4) \quad (7)$$

$$i_{La} = \frac{V_0}{L_a}(t-t_4) \quad (8)$$

Figure. 9(e), represents the equivalent circuit of the proposed converter at Mode. 5

Mode 6: $t_5 < t < t_6$

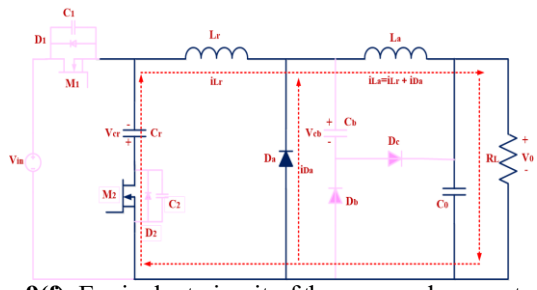


Fig. 9(f). Equivalent circuit of the proposed converter at Mode. 6.

At t_5, the ZVS conduction activates M_2, the auxiliary switch. Here, the resonant inductor L_r resonates with the resonant capacitor C_r, transferring its energy to it. The following expression describes the relationship between the resonant inductor's current i_{Lr}, voltage V_{Lr}, and capacitor voltage V_{Cr} [22]:

$$i_{Lr} = \frac{V_{in}}{Z_r}\sin\omega(t-t_5) \quad (9)$$

$$V_{Lr} = V_{in}\cos\omega(t-t_5)$$

$$V_{cr} = V_{in}[1-\cos\omega(t-t_5)] \quad (10)$$

Where the characteristic impedance is $Z_r = \sqrt{L_r/C_r}$

The resonant frequency is $\omega = \sqrt{1/L_rC_r}$

Figure. 9(f), represents the equivalent circuit of the proposed converter at Mode. 6

Mode 7: $t_6 < t < t_7$

The resonant inductor L_r gives up its energy at time t_6. The current in the resonant inductor, i_{Lr}, then changes direction, and the capacitor C_r, lets go of its power through M_2 and L_r. This is how can show the current in the resonant inductor i_{Lr} and [26] the stored inductor i_{La}:

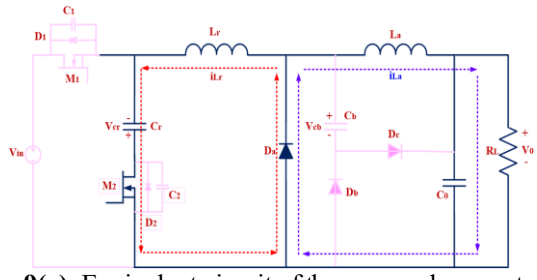


Fig. 9(g). Equivalent circuit of the proposed converter at Mode. 7.

$$i_{Lr} = \frac{V_{cr}}{L_r}(t-t_6) \quad (11)$$

$$i_{La} = \frac{V_0}{L_a}(t-t_6) \quad (12)$$

Figure. 9(g), represents the equivalent circuit of the proposed converter at Mode. 7

Mode 8: $t_7 < t < t_8$

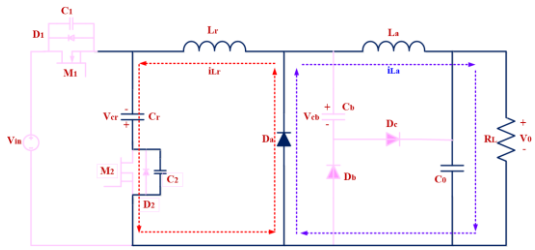


Fig. 9(h). Equivalent circuit of the proposed converter at Mode. 8.

The extra capacitance C_2 of the secondary switch M_2 is charged at time t_7 when it is turned off. The resonant capacitor C_r gives off energy through M_2 and L_r. This is how it can show the current in the resonant inductor i_{Lr} and the stored inductor [28] i_{La}:

$$i_{Lr} = \frac{V_{cr} - V_{DS2}}{L_r}(t - t_7) \tag{13}$$

$$i_{La} = \frac{V_0}{L_a}(t - t_7) \tag{14}$$

Figure. 9(h), represents the equivalent circuit of the proposed converter at Mode. 8

Mode 9: $t_8 < t < t_9$

When the auxiliary switch M_2 voltage V_{DS2} equals $V_{in} + V_{DS1} + V_{cr}$ at time t_8, the resonant inductor's current i_{Lr} will flow via the main switch's parasitic capacitance C_1. The parasitic capacitance C_1 of the key switch M_1 discharges at this interval. To accomplish ZVS for main switch M_1, resonant inductor L_r energy must fulfill the following inequality [28].:

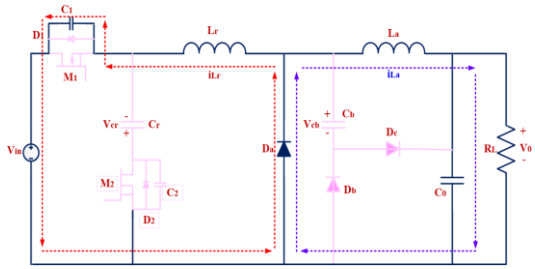


Fig. 9(i). Equivalent circuit of the proposed converter at Mode. 9.

$$\frac{1}{2}[i_{Lr}(t - t_8)]^2 L_r > \frac{1}{2}[V_{DS1}(t - t_8)]^2 C_1 \tag{15}$$

The current that is stored in the inductor, denoted by i_{La}, can be represented as follows:

$$i_{La} = \frac{V_0}{L_a}(t - t_8) \tag{16}$$

Figure. 9(i), represents the equivalent circuit of the proposed converter at Mode. 9

Mode 10: $t_9 < t < t_{10}$

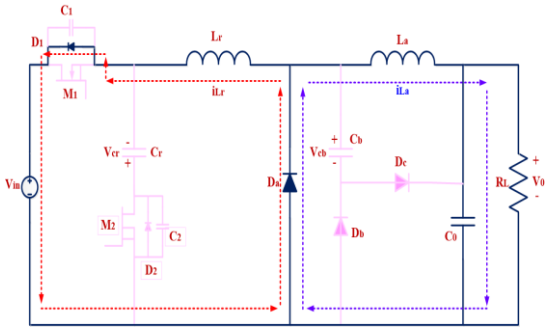


Fig. 9(j). Equivalent circuit of the proposed converter at Mode. 10.

The parasitic capacitance C_1 of the key switch M_1 discharges zero at t_9. The primary switch's body diode D_1 conducts due to the resonant inductor's current i_{Lr}, creating a ZVS characteristic. Currents i_{Lr} and i_{La} of the resonant and stored inductors are [31]:

$$i_{Lr} = \frac{V_{cr}}{L_r}(t - t_9) \tag{17}$$

$$i_{La} = \frac{V_0}{L_a}(t - t_9) \tag{18}$$

Figure. 9(j), represents the equivalent circuit of the proposed converter at Mode. 10

Mode 11: $t_{10} < t < t_{11}$

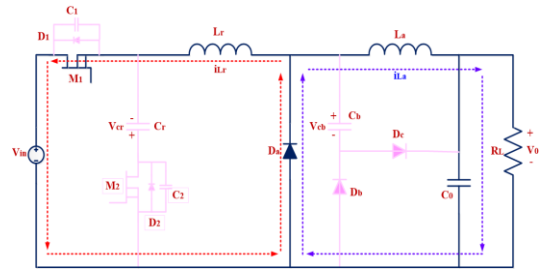


Fig. 9(k). Equivalent circuit of the proposed converter at Mode. 11.

At time t_{10}, the ZVS condition turns on M_1. If current in the resonant inductor, i_{Lr}, drops to zero at time t_{11}, it moves forward and flows from the L_r, C_b, D_c *and* R_L. Figure 9 shows a device that works like Mode 11. The soft-switching buck converter that was designed has gone through one switching cycle.

4. Selection of MPPT Method

The suggested technique of soft-switching buck converter for solar applications needs to have the best control strategy put in place to make sure it has a quick dynamic reaction and tall conversion efficiency. MPPT and the technique of soft-switching cells are the best ways to control something. This part goes over the choices for planning methods.

A buck converter with soft-switching cells will often use the ZVS features of active switches to cut down on switching losses and improve the efficiency of the conversion. An active switch, a resonant inductor, and a resonant capacitor are needed for the active soft-switching cell. A normal buck converter has different active soft-switching cell combos, which can be seen in Figure 8.

5. Simulation Results

5.1 Simulation Results for PV

Parameters used for simulating PV are
Voltage of Solare PV panel = 60-80 V
Output of PV Cell = <3 W and 0.5V

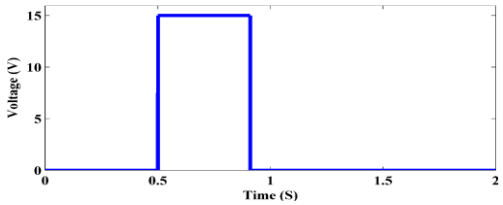


Fig. 11. Gate Signal Waveforms of switch M_1.

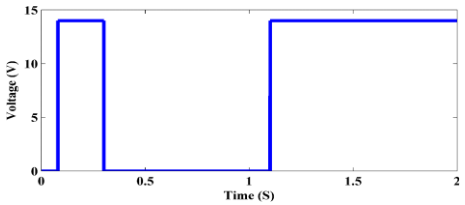


Fig. 12. Gate signal waveforms of switch M_2.

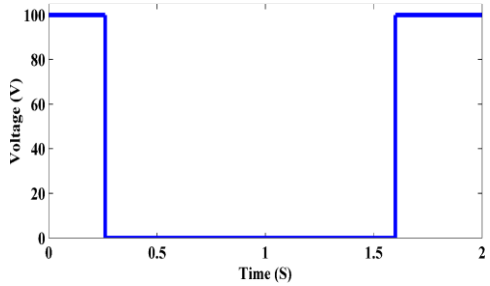


Fig. 13. Driving signal waveforms of switch M_1.

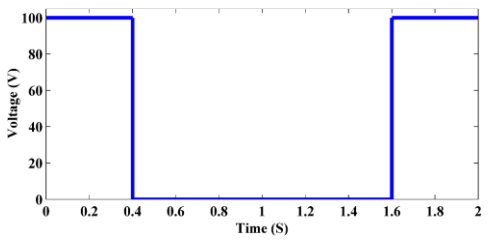


Fig. 14. Driving signal waveforms of switch M_2.

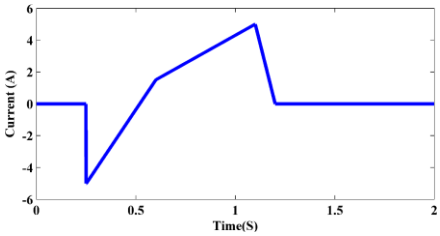


Fig. 15. Measured current waveform of switch M_1.

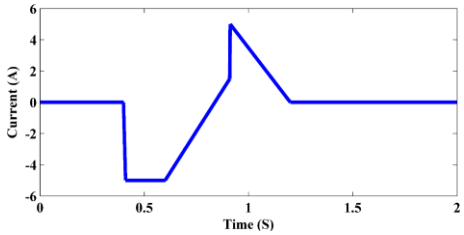


Fig. 16. Measured current waveform of switch M_2.

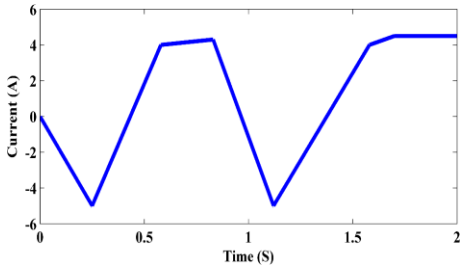


Fig. 17. The measured current waveform of switch M_1 at the resonant inductor.

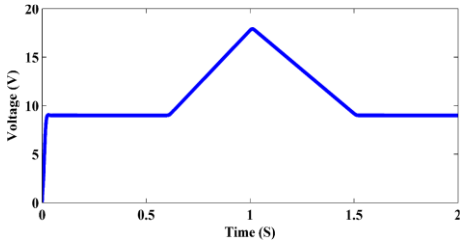


Fig. 18. Measured voltage waveform of switch M_1 at resonant inductor.

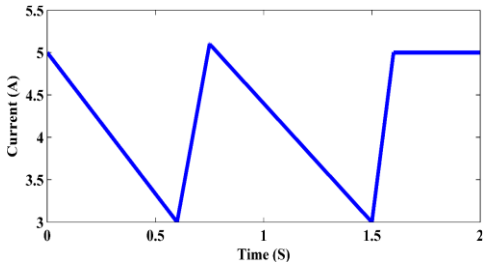


Fig. 19. Stored current waveform of the resonant inductor.

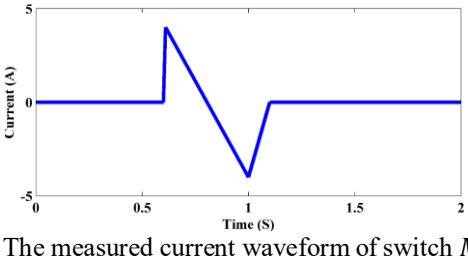


Fig. 20. The measured current waveform of switch M_1 at the resonant capacitor.

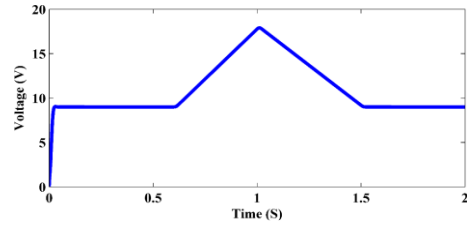


Fig. 21. Measured voltage waveform of switch M_1 at the resonant capacitor.

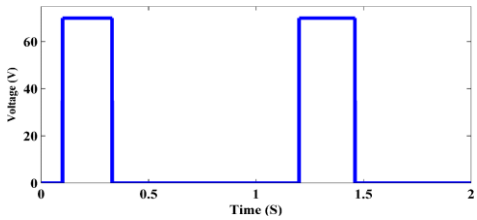


Fig. 22. Measured voltage waveform of the freewheeling diode.

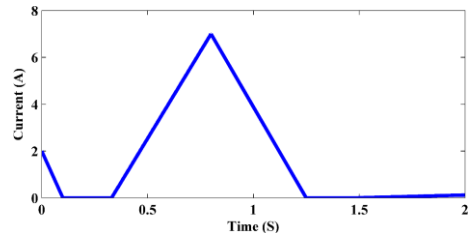


Fig. 23. Measured current waveform of freewheeling diode.

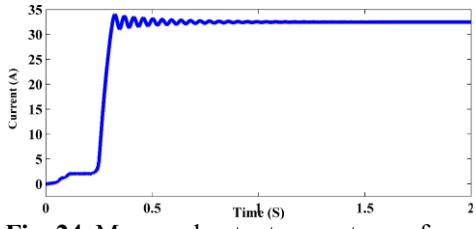


Fig. 24. Measured output current waveform.

5.2 Simulation Results for Fuel Cell

Parameters used for simulating fuel cells are
Open Circuit Voltage = 80V
Nominal Operating Current = 6A
Nominal Operating Voltage = 60A
Maximum Operating Current = 8A
Maximum Operating Voltage = 80V
Number of cells = 800
Operating temperature = 65^0C
Nominal Composition = (H_2, O_2, H_2O(Air)) = (99.95, 21, 1)
Operating temperature = 65^0C
Nominal Composition = (H_2, O_2, H_2O(Air)) = (99.95, 21, 1)

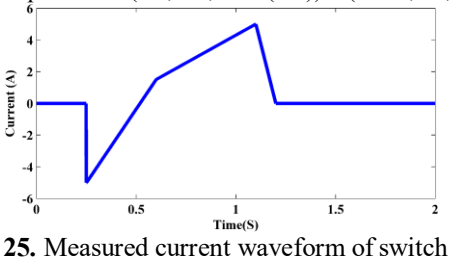


Fig. 25. Measured current waveform of switch M_1.

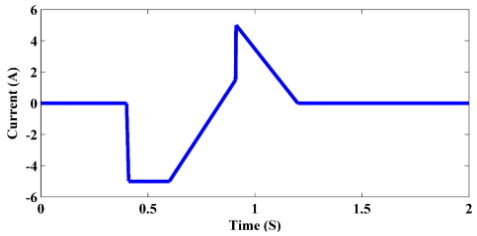


Fig. 26. Measured current waveform of switch M_2.

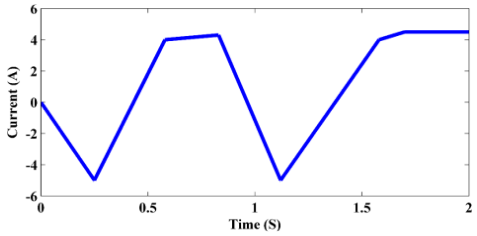


Fig. 27. Measured current waveform of switch M_1 at the resonant inductor.

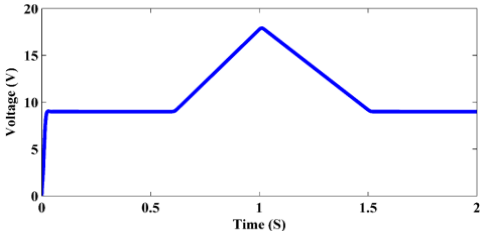


Fig. 28. Measured voltage waveform of switch M_1 at the resonant inductor.

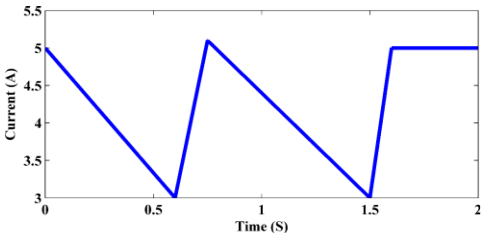


Fig. 29. Stored current waveform of the resonant inductor.

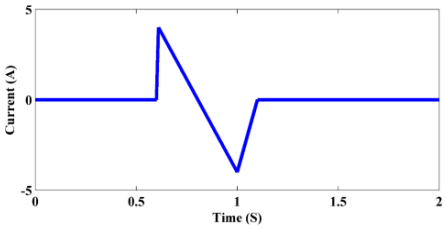


Fig. 30. The measured current waveform of switch M_1 at the resonant capacitor.

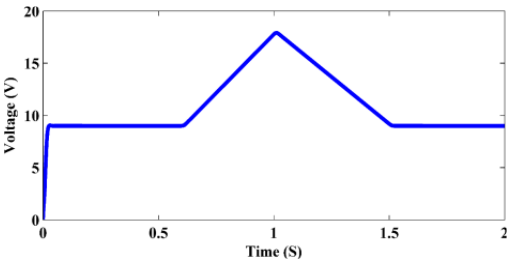


Fig. 31. Measured voltage waveform of switch M_1 at the resonant capacitor.

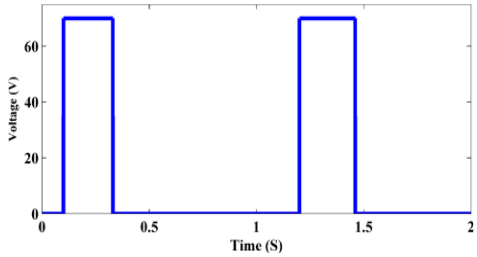


Fig. 32. Measured voltage waveform of the freewheeling diode.

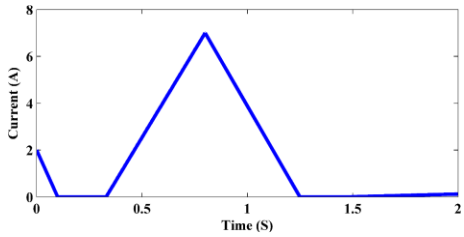


Fig. 33. Measured current waveform of freewheeling diode.

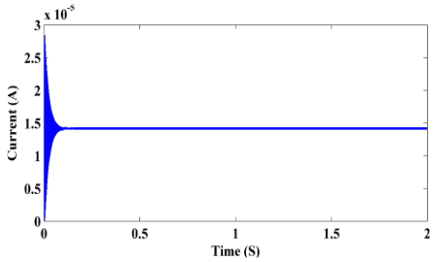


Fig. 34. Measured output current waveform.

5.3 Simulation Results for Battery

The parameters used for simulating the battery are
Type of Battery = Nickel-Metal-Hydride battery Nominal Voltage = 60-80 V
Rated Capacity = 6.5Ah

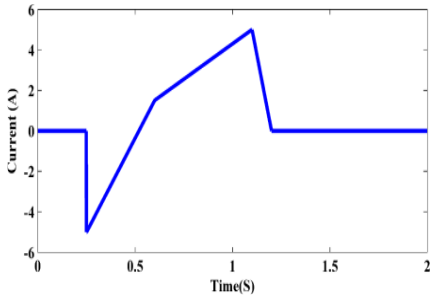


Fig. 35. Measured current waveform of switch M_1.

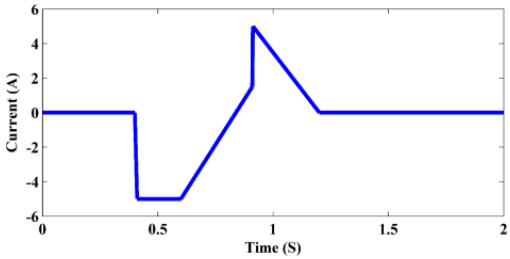


Fig. 36. Measured current waveform of switch M_2.

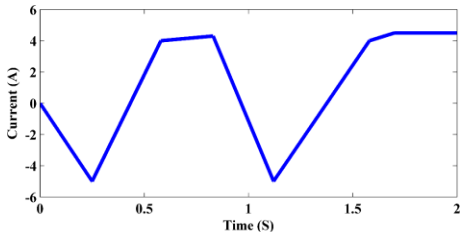


Fig. 37. The measured current waveform of switch M_1 at the resonant inductor.

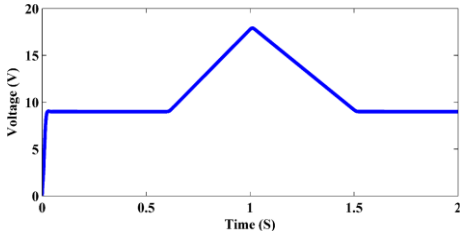


Fig. 38. Measured voltage waveform of switch M_1 at resonant inductor.

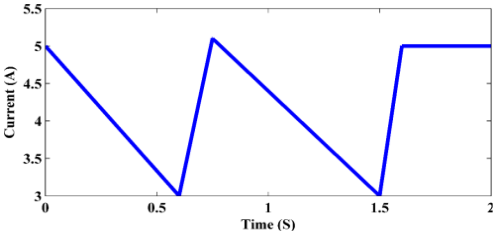


Fig. 39. Stored current waveform of the resonant inductor.

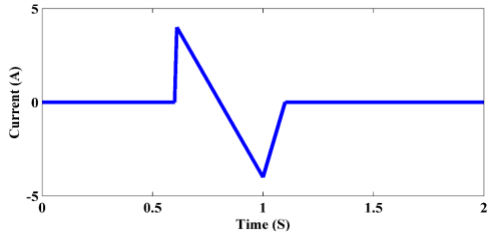


Fig. 40. The measured current waveform of switch M_1 at the resonant capacitor.

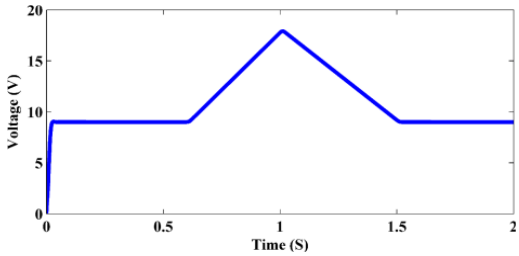


Fig. 41. Measured voltage waveform of switch M_1 at the resonant capacitor.

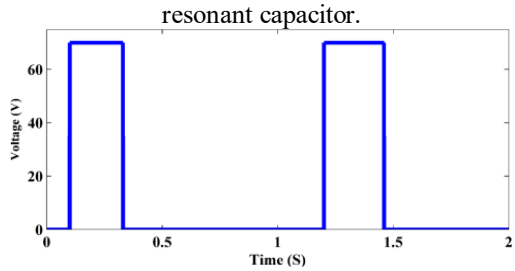


Fig. 42. Measured voltage waveform of a freewheeling diode.

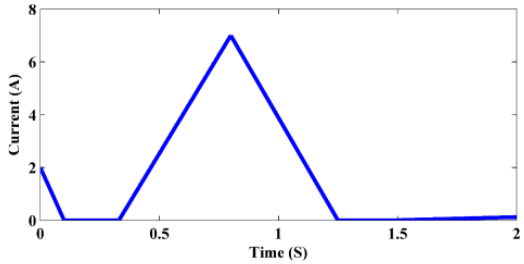


Fig. 43. Measured current waveform of freewheeling diode.

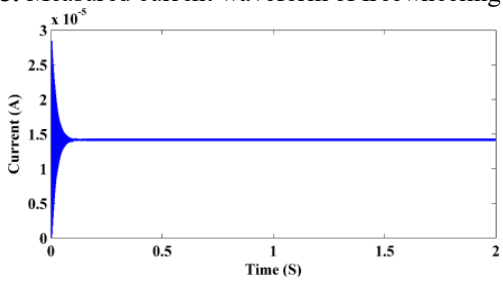


Fig. 44. Measured output current waveform.

6. Conclusion

By using soft switching, it became possible to fulfill the requirements for frequency converters that were high-power, high-efficiency, small footprint, low-interference, and low-loss. In this article, a comparison is made between various "soft switching" methods. The primary focus was on the categorization of soft-switching tactics that were utilized by families. To reduce switching losses during power on/off, the QRC, MRC, RTC, and ZTC families are being studied for ZVS/ZCS. However, this will expose the system to extremely high levels of voltage and current, which could be potentially hazardous. ZVT and ZCT make soft switching possible with minimal voltage and current stress on the primary switch, even though these converters may have challenges with voltage conversion range and changeable frequency. In this investigation, the article presents a buck converter that makes use of soft-switching cells and is designed to be utilized with solar panels on a large scale. A zero-voltage switching (ZVS) feature is present in both the main and assisting switches while they are in the on-state. Additionally, the reverse return current of the freewheeling diode can be throttled when the switch is in the off state. Thus, switching losses and electromagnetic interference (EMI) can be decreased in both the main switches and the auxiliary switches. Using simulation, the efficiency and performance of the soft-switching buck converter on renewable energy sources such as solar photovoltaics, fuel cells, and batteries were successfully validated. Consequently, the soft-switching buck converter has the potential to be utilized in photovoltaic panel systems, fuel cells, and batteries.

Acknowledgment

The authors extend their appreciation to Taif University, Saudi Arabia, for supporting this work through project number (TU-DSPP-2024-128)

Funding

This research was funded by Taif University, Saudi Arabia, Project No. (TU-DSPP-2024-128)

References

[1] S. Abbasian, M. Farsijani, M. Tavakoli Bina, and A. Shahirinia, "A nonisolated common-ground high step-up soft-switching DC-DC Converter With Single Active Switch," IEEE Trans. Ind. Electron., vol. 70, no. 6, pp. 5728–5738, 2023, doi: 10.1109/TIE.2022.3198262.

[2] Z. M'barki, K. S. Rhazi, and Y. Mejdoub, "A proposal of structure and control overcoming conducted electromagnetic interference in a buck converter," Int. J. Power Electron. Drive Syst., vol. 13, no. 1, pp. 380–389, 2022, doi: 10.11591/ijpeds.v13.i1.pp380-389.

[3] S. Abbasian, H. S. Gohari, M. Farsijani, K. Abbaszadeh, H. Hafezi, and S. Filizadeh, "Single-switch resonant soft-switching ultra-high gain DC-DC converter with continuous input current," IEEE Access, vol. 10, pp. 33482–33491, 2022, doi: 10.1109/ACCESS.2022.3161456.

[4] S. J. Gambhire, M. K. Kumar, K. Mallikarjuna, A. N. Venkateswarlu, C. N. Sai Kalyan and B. S. Goud, "Performance comparison of various classical controllers in LFC of hydro-thermal power system with time delays," 2022 10th International Conference on Smart Grid (icSmartGrid), Istanbul, Turkey, 2022, pp. 401-406, doi: 10.1109/icSmartGrid55722.2022.9848690.

[5] M. Gupta and A. Prem, "A pwm method for reducing dv/dt and switching losses in two-stage power converters," IEEE Trans. Ind. Appl., vol. 59, no. 4, pp. 4375–4386, 2023, doi: 10.1109/TIA.2023.3272540.

[6] H. Li, H. Du, Y. Zeng, Z. Qiu, X. Jiang, and Z. Chen, "A modified interleaved capacitor clamped dc-dc converter with non-resonant soft switching," IEEE Trans. Power Electron., vol. 37, no. 10, pp. 12221–12236, 2022, doi: 10.1109/TPEL.2022.3163010.

[7] G. S. Rao, B. S. Goud and C. R. Reddy, "Power quality improvement using ASO technique," 2021 9th International Conference on Smart Grid (icSmartGrid), Setubal, Portugal, 2021, pp. 238-242, doi: 10.1109/icSmartGrid52357.2021.9551226.

[8] R. Faraji, L. Ding, T. Rahimi, and M. Kheshti, "Application of soft-switching cell with inherent redundancy properties for enhancing the reliability of boost-based DC-DC converters," IEEE Trans. Power Electron., vol. 36, no. 11, pp. 12342–12354, 2021.

[9] M. Venkatesh, "A review on the estimate solar pv cell variables for efficient photovoltaic systems," Int. J. Smart grid, vol. 7, no. V7i3, 2023, doi: 10.20508/ijsmartgrid.v7i3.286.g291.

[10] C. R. Reddy, B. S. Goud, B. N. Reddy, M. Pratyusha, C. V. Vijay Kumar and R. Rekha, "Review of islanding detection parameters in smart grids," 2020 8th International Conference on Smart Grid (icSmartGrid), Paris, France, 2020, pp. 78-89, doi: 10.1109/icSmartGrid49881.2020.9144923.

[11] C. Rao, A. Hajjiah, M. A. El-Meligy, M. Sharaf, A. T. Soliman, and M. A. Mohamed, "A novel high-gain soft-switching DC-DC converter with improved PO MPPT for photovoltaic applications," IEEE Access, vol. 9, pp. 58790–58806, 2021, doi: 10.1109/ACCESS.2021.3072972.

[12] K. V. G. Rao, M. Kiran Kumar, and B. Srikanth Goud, "An independently controlled two output half bridge resonant LED driver," Electr. Power Components Syst., vol. 0, no. 0, pp. 1–21, 2023, doi: 10.1080/15325008.2023.2238695.

[13] S. Hasanpour, M. Forouzesh, Y. Siwakoti, and F. Blaabjerg, "A novel full soft- switching high-gain DC/DC converter based on three-winding coupled-inductor," IEEE Trans. Power Electron., vol. 36, no. 11, pp. 12656–12669, 2021, doi: 10.1109/TPEL.2021.3075724.

[14] S. Natarajan, T. Sudhakar Babu, K. Balasubramanian, U. Subramaniam, and D. J. Almakhles, "A state-of-the-art review on conducted electromagnetic interference in non-isolated DC to DC converters," IEEE Access, vol. 8, pp. 2564–2577, 2020, doi: 10.1109/ACCESS.2019.2961954.

[15] K. Venkata Govardhan Rao, M. K. Kumar, B. S. Goud, M. Bajaj, M. Abou Houran, and S. Kamel, "Design of a bidirectional DC/DC converter for a hybrid electric drive system with dual-battery storing energy," Front. Energy Res., vol. 10, no. November, 2022, doi: 10.3389/fenrg.2022.972089.

[16] Mirzaei and M. Rezvanyvardom, "High voltage gain soft switching full bridge interleaved Flyback DC-DC converter for PV applications," Sol. Energy, vol. 196, no. June 2019, pp. 217–227, 2020, doi: 10.1016/j.solener.2019.11.032.

[17] H. Oufettoul, S. Motahhir, I. A. Abdelmoula, G. Aniba, W. Issa and O. Mahir, "Optimum MPPT technique for reconfiguring the photovoltaic array under partial shading failure," 2023 12th International Conference on Renewable Energy Research and Applications (ICRERA), Oshawa, ON, Canada, 2023, pp. 331-338, doi: 10.1109/ICRERA59003.2023.10269423.

[18] B. S. Goud, B. L. Rao, "Power quality enhancement in grid-connected PV/Wind/Battery using UPQC: Atom search optimization," J Electr Eng Technol. 2021;16(2):821–35.

[19] K. Sayed, M. G. Gronfula, and H. A. Ziedan, "Novel soft-switching integrated boost DC- DC converter for PV power system," Energies, vol. 13, no. 3, 2020.

[20] K. V. G. Rao and M. K. Kumar, "The harmonic reduction techniques in shunt active power filter when integrated with non-conventional energy sources," Indones. J. Electr. Eng. Comput. Sci., vol. 25, no. 3, pp. 1236–1245, 2022, doi: 10.11591/ijeecs.v25.i3.pp1236-1245.

[21] S. R. Arya, and J. Gupta, "Solar PV array-based DC–DC converter with MPPT for low power applications," Renew. Energy Focus, vol. 34, no. 00, pp. 109–119, 2020, doi: 10.1016/j.ref.2020.05.003.

[22] A. Subramanian and U. Govindarajan, "Analysis and mitigation of conducted EMI in current mode controlled DC-DC converters," IET Power Electron., vol. 12, no. 4, pp. 667–675, 2019, doi: 10.1049/iet-pel.2018.5322.

[23] K. V. G. Rao, M. K. Kumar, B. S. Goud, T. A. Devi, G. S. Rao, A. Giriprasad, I. Prashanth, T. V. S. Kalyani, "A new brushless DC motor driving resonant pole inverter optimized for batteries," Int. J. Power Electron. Drive Syst., vol. 14, no. 4, pp. 2021–2031, 2023, doi: 10.11591/ijpeds.v14.i4.pp2021-2031.

[24] F. M. Etemadi, and A. Baghramian, "A new high-step-up DC-DC converter using three-windings transformer and soft-switching for use in photovoltaic systems," 2019 10th Int. Power Electron. Drive Syst. Technol. Conf. PEDSTC 2019, pp. 207–212, 2019, doi: 10.1109/PEDSTC.2019.8697846.

[25] K. Umadevi and C. Nagarajan, "Design and implementation of novel soft switching method based DC-DC converter with non-isolated coupled inductor in solar system using FPGA," Microprocess. Microsyst., vol. 73, p. 102952, 2020, doi: 10.1016/j.micpro.2019.102952.

[26] A. Ariyan and M. R. Yazdani, "Zero-voltage-transition buck converter for high step-down DC-DC conversion with low EMI," J. Power Electron., vol. 17, no. 6, pp. 1445–1453, 2017, doi: 10.6113/JPE.2017.17.6.1445.

[27] A. Subramanian and U. Govindarajan, "Analysis and mitigation of EMI in DC-DC converters using QR interaction," IET Circuits, Devices Syst., vol. 11, no. 4, pp. 371–380, 2017, doi: 10.1049/iet-cds.2016.0288.

[28] N. Sudhakar, N. Rajasekar, and A. Shanmuga Sundari, "FPGA based Chaotic PWM combined with soft switching for effective EMI mitigation in boost converter," 2016 Int. Conf. Energy Effic. Technol. Sustain. ICEETS 2016, pp. 148–152, 2016, doi: 10.1109/ICEETS.2016.7582915.

[29] B. S. Goud, C. N. S. Kalyan, D. Krishna, B. N. Reddy, M. Bajaj, S. Choudhury, S. Shukla, "Power quality enhancement in PV integrated system using GSA-FOPID CC-VSI controller," EAI Endorsed Trans Scalable Inf Syst. 2023;10(6):1–6.

[30] D. Jiang, Z. Wang, W. Chen, J. Liu, X. Zhao, and W. Sun, "Common-mode electromagnetic interference mitigation for solid-state transformers," Chinese J. Electr. Eng., vol. 8, no. 3, pp. 22–36, 2022.

[31] Z. M'barki, K. S. Rhazi, and Y. Mejdoub, "A novel fuzzy logic control for a zero current switching-based buck converter to mitigate conducted electromagnetic interference," Int. J. Electr. Comput. Eng., vol. 13, no. 2, pp. 1423–1436, 2023, doi: 10.11591/ijece.v13i2.pp1423-1436.

[32] K. A. M. Junaid, Y. Sukhi, N. Anjum, Y. Jeyashree, A. F. Ahamed, S. Debbarma, G. Chaudhary, S.

Priyadarshini, N. Shylashree, S. Garg, V.Nath, "PV-based DC-DC buck-boost converter for LED driver," e-Prime - Adv. Electr. Eng. Electron. Energy, vol. 5, no. March, p. 100271, 2023, doi: 10.1016/j.prime.2023.100271.

[33] M. Gupta and A. Prem, "A PWM method for reducing dv/dt and switching losses in two-stage power converters," IEEE Trans. Ind. Appl., vol. 59, no. 4, pp. 4375–4386, 2023.